# COMPLEX *LOW*-PASS FILTERS

*Péter Kiss, Vladimir Prodanov, and Jack Glas*

Department of Communications Circuits Research, Agere Systems
600 Mountain Avenue, Murray Hill, NJ 07974, kpeter@agere.com

**ABSTRACT:** Quadrature zero-if transceivers suffer from the imbalance of the I and Q paths. By using a complex *low*-pass filter topology instead of a conventional pair of real low-pass filters, this imperfection can be reduced. Both analytical and numerical analysis show that the proposed technique is significantly more robust to circuit imperfections than the traditional architecture.

## 1. MOTIVATION

The performance of practical quadrature direct-conversion (zero-if) transceivers (Fig. 1.(a)), among other imperfections, suffers from I/Q imbalance caused by the mismatch of the mixers and the imperfect quadrature signals from the local oscillators [1, 2]. In addition, the mismatch between the frequency responses of the two real low-pass filters ($\text{LPF}_1$ and $\text{LPF}_2$ in Fig. 1.(a)) also contributes to the I/Q imbalance of the receiver, causing performance degradation. When zero-if topology is proposed for wide-band applications with more stringent requirements (e.g., 802.11a where $SNR \cong 30$ dB) then this distortion needs to be taken into account.

In this paper a single complex low-pass filter ($\text{LPF}_c$ in Fig. 1.(b)) is proposed to reduce the I/Q imbalance due to the two-path filtering. Complex filters has been discussed for many years [3]. In the late 1960-s, analog polyphase filters were proposed for single-sideband generators [4] and receivers [5]. About a decade later, their synthesis and analysis led to new developments [6–8]. Currently they are often used in low-if receiver ICs, e.g., [9–11].

Complex *low*-pass filters are a particular case of the popular complex *band*-pass filters [3–11]; however, the technical literature does not talk about them. Here, after a brief review of basic concepts, a detailed sensitivity analysis of such filters will be provided. It demonstrates that complex low-pass filters outperform the pair of real low-pass filters from I/Q imbalance point of view.

## 2. REAL FILTERS

In a conventional zero-if architecture [1,2], $\text{LPF}_1$ and $\text{LPF}_2$ form a two-input two-output linear network with complex input $x_c(t) \doteq x_1(t) + j\,x_2(t)$ and complex output $y_c(t) \doteq y_1(t) + j\,y_2(t)$ (Fig. 1.(a)). $X_p(\omega)$ and $X_n(\omega)$ denote the positive and negative frequency content of $X_c(\omega)$, respectively. Usually, $X_p(\omega)$ and $X_n(\omega)$ correspond to the desired signal and the undesired image, respectively (Fig. 3.(b)). If the transfer functions of $\text{LPF}_1$ and $\text{LPF}_2$ are defined as $H_1(\omega) = \frac{B_1(\omega)}{A_1(\omega)}$ and $H_2(\omega) = \frac{B_2(\omega)}{A_2(\omega)}$, then

$$\begin{aligned} Y_c(\omega) &= \frac{A_2(\omega)\,B_1(\omega) + A_1(\omega)\,B_2(\omega)}{2\,A_1(\omega)\,A_2(\omega)}(X_1(\omega) + j\,X_2(\omega)) \\ &\quad + \frac{A_2(\omega)\,B_1(\omega) - A_1(\omega)\,B_2(\omega)}{2\,A_1(\omega)\,A_2(\omega)}(X_1(\omega) - j\,X_2(\omega)) \\ &= H_{cm}(\omega)\,X_c(\omega) + H_{df}(\omega)\,X_c^*(-\omega). \end{aligned} \quad (1)$$

Published: IEEE ISCAS, Phoenix, AR, 27 May 2002, pp. I.525–I.528.

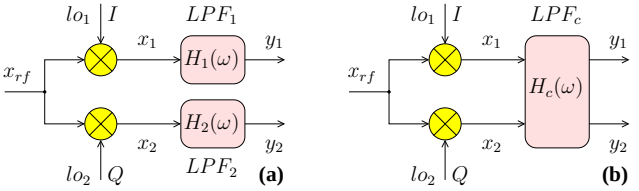


**Fig. 1**. Quadrature direct conversion receiver with **(a)** two real low-pass filters; **(b)** one complex low-pass filter.

Eq. (1) shows that the input complex signal $x_c(t)$ is processed in a parallel fashion by $h_{cm}(t)$ and $h_{df}(t)$ (Fig. 2.(a)). The common component of $H_1(\omega)$ and $H_2(\omega)$ forms $H_{cm}(\omega)$ which gives the desired (direct) output $H_{cm}(\omega) \cdot X_c(\omega)$. However, if $H_1(\omega)$ and $H_2(\omega)$ are not identical, then a nonzero $H_{df}(\omega)$ contributes to a leaked (undesired or difference) output component $H_{df}(\omega) \cdot X_c^*(-\omega)$. This means that a fraction of the positive-frequency signal $X_p(\omega)$ will be transformed into a negative-frequency signal $X_p^*(-\omega)$ which leaks to the top of $X_n(\omega)$ and distorts it (Fig. 3). Similarly, a fraction of $X_n^*(-\omega)$ distorts $X_p(\omega)$.

Note that this distortion occurs even if the complex local oscillator signal $lo_c$ is a single complex tone at $-\omega_{lo}$, as it was assumed in Fig. 3.(b). In practical situations, when $lo_c$ is not a perfect quadrature, then the effects of both imperfections add.

## 3. COMPLEX FILTERS

A complex filter is a two-input two-output linear network which frequency response is not necessarily symmetrical with respect to dc ($\omega = 0$). Its gain and phase responses are functions both of the frequency and the relative phase difference of the two real inputs $x_1$ and $x_2$ (Fig. 1.(b)).

As an example, a fourth-order all-pole band-pass complex filter with bandwidth $BW$ centered around $\omega_{if}$ is shown in Fig. 4.(a). Since $H_c(\omega)|_{\omega \in BW} \cong 0$ dB and $H_c(-\omega)|_{\omega \in BW} \ll 0$ dB, the complex band-pass filter provides image rejection in addition to filtering — without adding significantly to the hardware complexity of the filter.

A complex low-pass filter is a particular case of the popular complex band-pass filter when $\omega_{if} = 0$ (Fig. 4.(b)). Note that every complex pole is doubled and one of them is cancelled by a

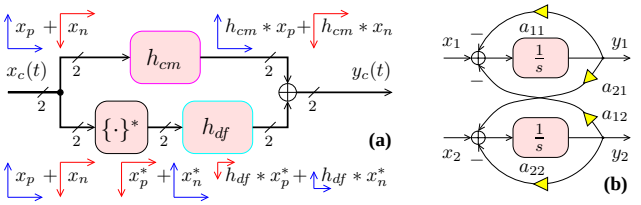


**Fig. 2**. **(a)** Parallel model of an imperfect low-pass filtering operation. **(b)** Implementation of a "single" complex pole.

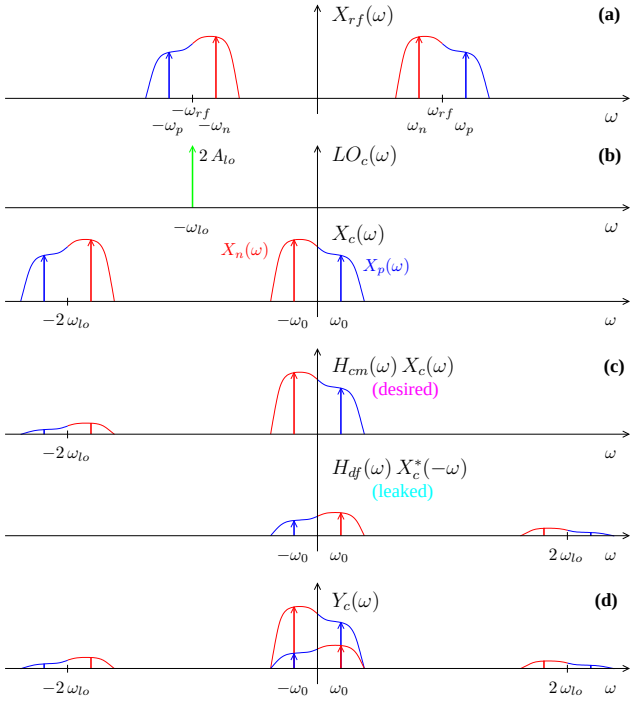


**Fig. 3**. Signal processing: **(a)** rf signal; **(b)** ideal I/Q mixing; **(c)** filtering: desired and leaked signals; **(d)** distorted output signal.

complex zero. The ideal response of such a filter can be designed to be identical with the ideal response of the pair of $\text{LPF}_1$ and $\text{LPF}_2$.

### 3.1. "Single" complex pole

The circuit implementation of complex filters involves realizing non-complex-conjugate (single) complex poles. This can be achieved by a pair of complex conjugate poles out of which one is cancelled by a single complex zero [6] (Fig. 4).

A "single" complex pole can effectively implemented using two integrators within a feedback loop with two inputs and two outputs [8] (Fig. 2.(b)). The complex output becomes

$$Y_c(s) \doteq \frac{s+a_{22}+j\,a_{21}}{D(s)}\,X_1(s) + \frac{s+a_{11}+j\,a_{12}}{D(s)}\,j\,X_2(s) \quad (2)$$

where $D(s) = s^2 + (a_{11}+a_{22})\,s + a_{11}a_{22} + a_{12}a_{21}$. In ideal case, i.e., $a_{11} = a_{22} = a$ and $a_{12} = a_{21} = b$, eq. (2) becomes

$$\begin{aligned} Y_{cid}(s) &= \frac{s+a+j\,b}{(s+a+j\,b)(s+a-j\,b)}\,(X_1(s)+j\,X_2(s)) \\ &= \frac{1}{s+a-j\,b}\,X_c(s) \;=\; H_{id1}(s)\,X_c(s) \end{aligned} \quad (3)$$

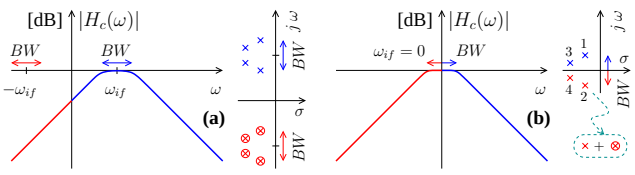


**Fig. 4**. Frequency response and pole-zero constellation for a 4th-order **(a)** complex band-pass filter; **(b)** complex low-pass filter.

Eq. (3) shows that the first-order ideal complex filter $H_{id1}(s)$ implements a "single" complex pole $p = -a + j\,b$, based on a perfect pole cancellation by the zero $z = -a - j\,b$.

Due to circuit imperfections, usually $a_{11} \neq a_{22} \neq a$ and $a_{12} \neq a_{21} \neq b$, so the pole-zero cancellation does not hold completely. Eq. (2) can be written as follows (similar to [12, p. 58])

$$\begin{aligned} Y_c(s) &= \frac{s+\frac{a_{11}+a_{22}}{2}+j\,\frac{a_{12}+a_{21}}{2}}{D(s)}\,(X_1(s)+j\,X_2(s)) \\ &\quad + \frac{\frac{a_{11}-a_{22}}{2}+j\,\frac{a_{12}-a_{21}}{2}}{D(s)}\,(X_1(s)-j\,X_2(s)) \\ &= H_{cm}(s)\,X_c(s) + H_{df}(s)\,X_c^*(s^*) \quad (4) \\ \Rightarrow\quad Y_c(\omega) &= H_{cm}(\omega)\,X_c(\omega) + H_{df}(\omega)\,X_c^*(-\omega) \quad (5) \end{aligned}$$

Since this last result is identical with eq. (1), a complex filter behaves in the same way as a pair of real filters, so it can be modeled by Fig. 2.(a). Also, a mismatched complex filter causes distortion as explained earlier and illustrated by Fig. 3. However, note that $H_{cm}(\omega)$ and $H_{df}(\omega)$ have real coefficients in eq. (1), but they have complex ones in eq. (5).

The coefficients $a_{11}$, $a_{12}$, $a_{21}$ and $a_{22}$ in Fig. 2.(b) are realized by various circuit elements depending on their implementations (e.g., passive $R$-$C$ [5], active $R$-$C$ [8], $g_m$-$C$ [11], etc.). Here, a normally-distributed error with $1\%$ variance was considered for each coefficient; the errors were assumed to be uncorrelated. Therefore, the magnitude and distribution of the errors need to be tailored to the specifics of the implementation.

The **simulated** behavior of an imperfect *versus* perfect single complex pole is shown in Fig. 5 (similar plots can be found in [12, p. 59]). The ideal pole-zero constellation presents a perfect pole-zero cancellation, and the frequency response $H_{id}(\omega)$ looks as expected. In the presence of $5\%$ errors[1] the poles $p_1$ and $p_2$ of the filter move away from the ideal value of $p$ which leads to a nonzero $H_{df}(s)$. However, the pole-zero cancellation within $H_{cm}(s)$ occurs at a high degree.

Note that the simulations were performed using a *black-box* approach. In this method a perfect quadrature complex signal, i.e., $x_c(t) = A\cos(\omega_0\,t) + j\,A\sin(\omega_0\,t)$, was applied to the input of the filter. The FFT of the resulting complex output $y_c(t)$ was

[1] In Figs. 5 and 8 the errors were kept larger than the practical value of $1\%$ in order to show meaningful pole-zero constellations.

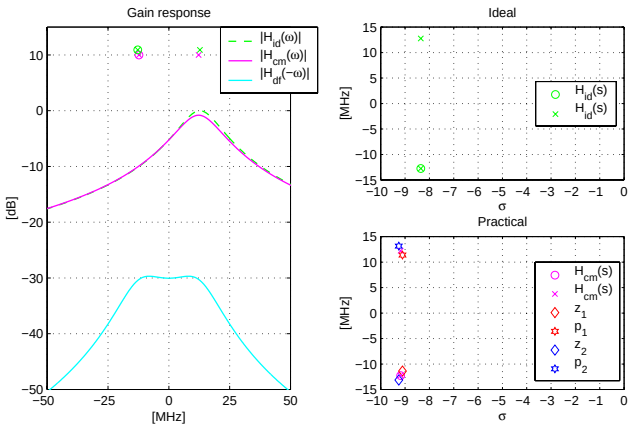


**Fig. 5**. First-order complex band-pass filter with $f_{if} = 13$ MHz and $\sigma_n = 5\%$ mismatch; $z_1 = -a_{11} - j\,a_{12}$, $p_1 = -a_{11} + j\,a_{12}$, $z_2 = -a_{22} - j\,a_{21}$, and $p_2 = -a_{22} + j\,a_{21}$.

measured at $\omega_0$ and $-\omega_0$, providing the values for $H_{cm}(\omega_0)$ and $H_{df}(-\omega_0)$, respectively. The experiment was performed for all the range of frequencies of interest. In addition, the transfer functions $H_{cm}(\omega)$ and $H_{df}(\omega)$ were calculated based on eq. (4). The numerical and analytical results were identical which proved the validity of the model described by eq. (4). Eqs. (6) and (7), defined and discussed later, were verified and validated by a similar simulation procedure.

## 4. CASCADE OF FILTERS

For a pair of real low-pass filters, eq. (1) holds for any order of the filters since there is no interaction between the individual I and Q stages but only at the global output (Fig. 2.(a)). On the other hand, for a cascade of complex filters the desired (direct) and undesired (leaked) signal components interact at the output of every stage. (Ladder filters will be discussed in an upcoming paper.)

Let us consider a fourth-order low-pass complex filter (Fig. 4.(b)), implemented as a cascade of "single" complex poles modeled in Fig. 6. Every of the four stages processes its complex input and provides desired and undesired output according to eq. (5) and illustrated by simulation results in Fig. 5. Due to this leakage mechanism, the image signal component of the input leaks into the desired signal, and vice versa. Moreover, the signal may leak more than *once* contributing accordingly to the global transfer functions.

Therefore,

$$\begin{aligned} H_{cm}(s) &= H_{cm4}(s)\,H_{cm3}(s)\,H_{cm2}(s)\,H_{cm1}(s) \\ &\quad + H_{df4}(s)\,H^*_{df3}(s^*)\,H_{cm2}(s)\,H_{cm1}(s) + \ldots \quad (6) \\ H_{df}(s) &= H_{df4}(s)H^*_{cm3}(s^*)H^*_{cm2}(s^*)H^*_{cm1}(s^*) \\ &\quad + H_{cm4}(s)H_{df3}(s)H^*_{cm2}(s^*)H^*_{cm1}(s^*) \\ &\quad + H_{cm4}(s)\,H_{cm3}(s)\,H_{df2}(s)\,H^*_{cm1}(s^*) \\ &\quad + H_{cm4}(s)\,H_{cm3}(s)\,H_{cm2}(s)\,H_{df1}(s) + \ldots \quad (7) \end{aligned}$$

$H_{cm}(\omega)$ and $H_{df}(\omega)$ contain even and odd numbers of time-domain complex conjugate operations on the input signal $x_c(t)$, respectively.

### 4.1. Complex *vs.* real low-pass filters

Replacing a pair of real low-pass filters $\text{LPF}_1$ and $\text{LPF}_2$ (RLPF) with a single complex low-pass filter (CLPF) in a quadrature direct-conversion receiver (Figs. 1.(a) *versus* (b)) is motivated by the expected increased robustness of the latter. A comparative sensitivity analysis will be presented in the following.

As an example, two imperfect RLPF and CLPF are compared in Fig. 8. Without loss of generality, both are fourth-order 8.5-MHz Chebyshev all-pole filters with a pass-band ripple of $R_p$ =

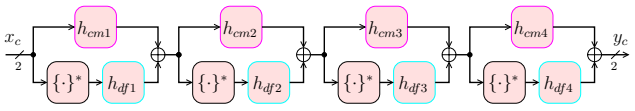


**Fig. 6**. Parallel model for a cascade of imperfect complex poles.

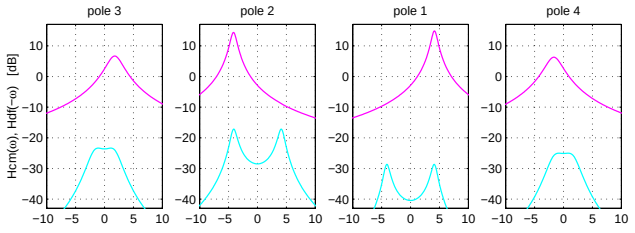


**Fig. 7**. Simulation example for a cascade of four complex stages.

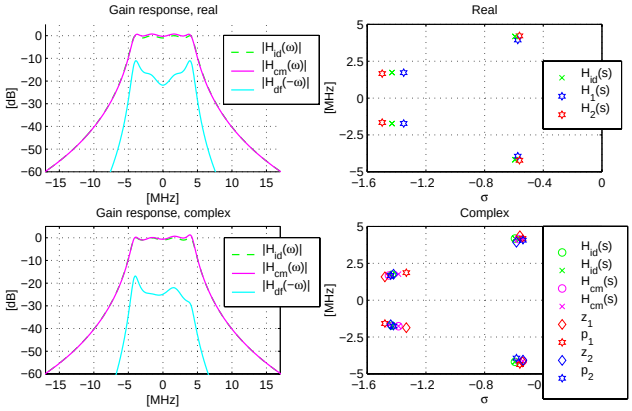


**Fig. 8**. RLPF *versus* CLPF for $N = 4$th order.

1 dB. They are affected by a normally distributed error with $\sigma_n = 5\%$, so their poles lay in clusters around the ideal locations. For the filters (i.e., $\text{LPF}_1$, $\text{LPF}_2$ and CLPF) cascade (as opposed to, e.g., ladder) implementations were assumed. One can define the average image-rejection ratio over a bandwidth $BW$ as

$$IMR = 10\,\log_{10} \int_{\omega \in BW} \left( \left| \mathcal{F}\left\{ \frac{h_{cm}(t)}{h_{df}(t)} \right\} \right| \right)^2 d\omega \quad [\text{dB}], \tag{8}$$

which shows how effectively a complex filter passes signal inputs while rejecting image inputs [12, p. 59]. The RLPF and CLPF lead to $IMR_r = 15.8$ dB and $IMR_c = 23.0$ dB, respectively. Therefore, the complex filter is 7.2 dB better than the real filters. However, these are just partial results. In order to draw general conclusions, the experiment presented in Fig. 8 was repeated for several mismatch states (as in a Monte-Carlo type analysis) and the results were processed statistically. Moreover, the effect of the sequence of stages was investigated — presented next.

### 4.2. Sequence of complex poles in CLPFs

The sequence of the stages plays a significant role in the complex filter's performance. From eq. (4) results that the magnitude of one stage's leakage is proportional to the distance to the origin (radius) of the pole it implements $R = \sqrt{a^2 + b^2}$. Usually, the pole with the highest $Q$, i.e., $Q = \frac{1}{2\,a}\sqrt{a^2 + b^2}$, has the largest radius $R$, but not always. (Here, the poles will be characterized by their $Q$-s rather than their $R$-s for simplicity.) Should the stages, therefore, be ordered in reverse sequence of their radius or pole Q-s?

In order to minimize the total leakage at the output of a cascaded complex low-pass filter the "leakage gain" seen by the most sensitive pole(s) needs to minimized. This is illustrated for a fourth-order filter in Fig. 7. The leakage of the pole 2 is given by $H_{df2}(\omega)$ which sees a leakage gain of $H^*_{cm3}(-\omega)H_{cm1}(\omega)H_{cm4}(\omega)$. This gain is evenly distributed for positive and negative frequencies, so it has the lowest possible average value. The same is true for the other high-Q pole 1. Next, this intuitive reason will be verified by numerical methods.

Fig. 9 presents the results of a statistical analysis. The variable $n$ indicates the sequence of stages (each stage implements an imperfect complex pole); the behavior of all $4! = 24$ possible permutations are shown. The poles are labeled $1 \ldots N$, sequenced in a decreasing order of their Q-s, but first the pole on the positive side comes, then that one on the negative side of $\omega$ follows (Fig. 4.(b)). The pole sequences corresponding to different $n$-s are given in Tab. 1. For example, $code(15) =$ 3-2-1-4 means that pole

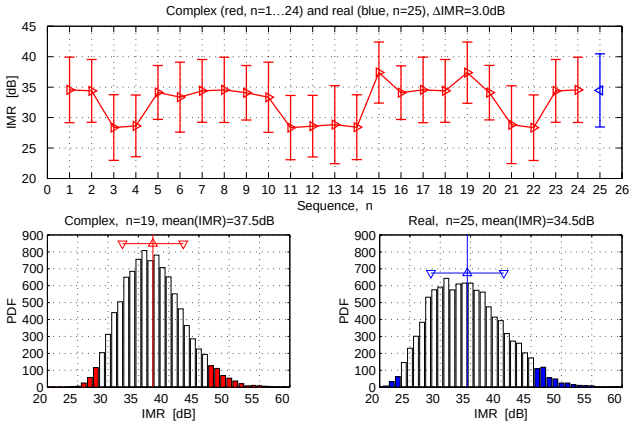


**Fig. 9**. The effect of ordering the poles in CLPF for $N = 4$.

3 is implemented in the first stage followed by pole 2, pole 1, and pole 4, like in Fig. 7. $n = 25$ is for RLPF. For each sequence $n$, a set of $10,240$ normally distributed ($\sigma_n = 1\%$) random mismatch states were simulated which error-bar (mean value and variance) is shown in Fig. 9. On the lower part of this figure, two histograms of $IMR$ are shown for $n = 19$ (CLPF) and $n = 25$ (RLPF), respectively. Note that CLPF has a narrower distribution than RLPF.

Based on the $IMR$ performance of CLPFs shown in Fig. 9, three categories of CLPFs can be clearly identified: "best" ($n \in \{15, 19\}$), "mediocre" ($n \in \{1, 2, 5–10, 16–18, 20, 23, 24\}$), and "worst" ($n \in \{3, 4, 11-14, 21, 22\}$). In the "best" group the poles follow a *shoestring* pattern. There are only two such sequences possible, i.e., $code(15)$ = 3-2-1-4 and $code(19)$ = 4-1-2-3 (Fig. 10.(a)). Indeed, these sequences minimize the "leakage gain" seen by the most sensitive poles. Finally, Fig. 9 shows that the best sequenced CLPFs achieve about 3 dB larger $IMR$ compared to RLPFs for $N = 4$. Note that this result depends on the highest value of the pole Q-s; for the filter in Fig. 8, $Q_{max} = 3.5$. If a ripple of 3 dB is assumed, which boosts up the $Q_{max}$ to 5.5, then $\Delta IMR$ becomes 4.1 dB. Therefore, the proposed technique is more effective for high-Q (i.e, more selective) filters.

The benefits of using CLPF over RLPF are better when the filter's order increases; note that higher-order filters are more likely to use high-Q poles. This is summarized in Tab. 2, e.g., the improvement is about 7 dB for $N = 8$. It was verified by simulations that in the case of higher-order filters, the above-described shoestring criteria for choosing the best sequence for CLPF remains valid. For example, for $N = 6$ the two best sequences should be 5-4-1-2-3-6 and 6-3-2-1-4-5 (Fig. 10.(b)). For odd-order filters, the position of the real pole does not matter much since its leakage is small and its response is symmetrical in respect to dc. For $N = 2$ and $N = 3$ the CLPF is unbalanced, and it performs pretty similar to the RLPF (Tab. 2). However, the practical significance of second- and third-order filters is less dramatic.

In summary, the intuitive and statistical analysis presented in this section demonstrated that it is possible to predict apriori the most robust CLPF topology. Also, it turns out that the CLPFs are significantly less sensitive to circuit imperfections than RLPFs.

| $n$ | $code(n)$ | $n$ | $code(n)$ | $n$ | $code(n)$ | $n$ | $code(n)$ |
|---|---|---|---|---|---|---|---|
| 1 | 1-2-3-4 | 7 | 2-1-3-4 | 13 | 3-1-2-4 | **19** | **4-1-2-3** |
| 2 | 1-2-4-3 | 8 | 2-1-4-3 | 14 | 3-1-4-2 | 20 | 4-1-3-2 |
| 3 | 1-3-2-4 | 9 | 2-3-1-4 | **15** | **3-2-1-4** | 21 | 4-2-1-3 |
| 4 | 1-3-4-2 | 10 | 2-3-4-1 | 16 | 3-2-4-1 | 22 | 4-2-3-1 |
| 5 | 1-4-2-3 | 11 | 2-4-1-3 | 17 | 3-4-1-2 | 23 | 4-3-1-2 |
| 6 | 1-4-3-2 | 12 | 2-4-3-1 | 18 | 3-4-2-1 | 24 | 4-3-2-1 |

**Table 1**. All 24 permutations of four poles.

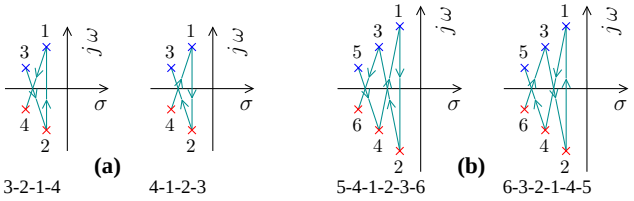


**Fig. 10**. Shoestring patterns of poles for **(a)** $N = 4$; **(b)** $N = 6$.

| $N$, order | 2 | 3 | 4 | 5 | 6 | 8 |
|---|---|---|---|---|---|---|
| $Q_{max}$ | 0.9 | 2.0 | 3.5 | 5.5 | 8.0 | 14.2 |
| $\overline{IMR_c}$ [dB] | 41.0 | 37.8 | 37.5 | 35.3 | 35.4 | 33.6 |
| $\overline{IMR_r}$ [dB] | 41.5 | 37.6 | 34.5 | 31.8 | 29.3 | 26.6 |
| $\Delta\overline{IMR}$ [dB] | **-0.5** | **0.2** | **3.0** | **3.5** | **6.1** | **7.0** |

**Table 2**. CLPF *versus* RLPF in function of $N$.

## 5. CONCLUSIONS

The proposed complex low-pass filter is a novel topology suitable for quadrature direct-conversion receivers. Detailed analytical and numerical analysis were presented. In order to reach maximal robustness for a complex low-pass filter, its stages should be ordered in an apriori predictable shoestring pattern. It turns out that the complex low-pass filters are several dBs more robust to circuit imperfections than the traditionally used real low-pass filters. Moreover, the proposed technique is even more effective for high-Q filters.

## 6. REFERENCES


[1] A. A. Abidi, "Direct-conversion radio transceivers for digital communications," *IEEE JSSC*, pp. 1399–1410, Dec. 1995.

[2] B. Razavi, "Design considerations for direct-conversion receivers," *IEEE JSSC*, pp. 428–435, June 1997.

[3] D. Gabor, "Theory of communication," *J. of the Institution of Electrical Engineers*, vol. 93, part III, pp. 429–457, 1946.

[4] M. J. Gingell, "A symmetrical polyphase network," U.S. Patent 3 559 042, June 7, 1968.

[5] M. J. Gingell, *The Synthesis and Application of Polyphase Networks with Sequence Asymmetric Properties*, Ph.D. thesis, Univ. of London, 1975. <http://users.vnet.net/gingell>

[6] G. R. Lang and P. O. Brackett, "Complex analogue filters," in *Proc. of the European Conference on Circuit Theory and Design*, 1981, pp. 412–419.

[7] W. M. Snelgrove and A. S. Sedra, "State-space synthesis of complex analog filters," in *Proc. of the European Conference on Circuit Theory and Design*, 1981, pp. 420–424.

[8] A. Sedra, W. Snelgrove, and R. Allen, "Complex analog bandpass filters designed by linearly shifting real low-pass prototypes," in *Proc. of ISCAS*, 1985, pp. III.1223–III.1226.

[9] J. Crols and M. S. Steyaert, "A single-chip 900 MHz CMOS receiver front-end with a high performance low-if topology," *IEEE JSSC*, pp. 1483–1492, Dec. 1995.

[10] S. A. Jantzi, K. W. Martin, and A. S. Sedra, "Quadrature bandpass delta-sigma modulation for digital radio," *IEEE JSSC*, pp. 1935–1950, Dec. 1997.

[11] V. Prodanov, G. Palaskas, J. Glas, and V. Boccuzzi, "A CMOS AGC-less IF strip for Bluetooth," *ESSCIRC*, 2001.

[12] S. A. Jantzi, *Quadrature Bandpass Delta-Sigma Modulation for Digital Radio*, Ph.D. thesis, Univ. of Toronto, 1997.